ISSN 8755-6839

SCIENCE OF TSUNAMI HAZARDS

Journal of Tsunami Society International

Volume 30 Number 1 2011

THE RESPONSE OF MONTEREY BAY TO THE 2010 CHILEAN EARTHQUAKE

Laurence C. Breaker[1], T. S. Murty[2], Stephanie J. Flora[1] and Craig N. Hunter[1]

[1] Moss Landing Marine Laboratories, Moss Landing, CA 95039
[2] University of Ottawa, Ottawa, Canada

ABSTRACT

The primary frequencies contained in the arrival sequence produced by the tsunami from the Chilean earthquake of 2010 in Monterey Bay were extracted to determine the seiche modes that were produced. Singular Spectrum Analysis (SSA) and Ensemble Empirical Mode Decomposition (EEMD) were employed to extract the primary frequencies of interest. The wave train from the Chilean tsunami lasted for at least four days due to multipath arrivals that may not have included reflections from outside the bay but most likely did include secondary undulations, and energy trapping in the form of edge waves, inside the bay.

The SSA decomposition resolved oscillations with periods of 52-57, 34-35, 26-27, and 21-22 minutes, all frequencies that have been predicted and/or observed in previous studies. The EEMD decomposition detected oscillations with periods of 50-55 and 21-22 minutes. Periods in the range of 50-57 minutes varied due to measurement uncertainties but almost certainly correspond to the first longitudinal mode of oscillation for Monterey Bay, periods of 34-35 minutes correspond to the first transverse mode of oscillation that assumes a nodal line across the entrance of the bay, a period of 26-27 minutes, although previously observed, may not represent a fundamental oscillation, and a period of 21-22 minutes has been predicted and observed previously. A period of ~37 minutes, close to the period of 34-35 minutes, was generated by the Great Alaskan Earthquake of 1964 in Monterey Bay and most likely represents the same mode of oscillation. The tsunamis associated with the Great Alaskan Earthquake and the Chilean Earthquake both entered Monterey Bay but initially arrived outside the bay from opposite directions. Unlike the Great Alaskan Earthquake, however, which excited only one resonant mode inside the bay, the Chilean Earthquake excited several modes suggesting that the asymmetric shape of the entrance to Monterey Bay was an important factor and that the directions of the incoming tsunami-generated waves were most likely different.

The results from SSA and EEMD produced results that differed. Although a period of 34-35 minutes was observed in the SSA, it was not detected in the EEMD. In previous comparisons, however, we have observed that oscillations detected in EEMD were not detected in SSA. SSA also revealed an oscillation with a period of 26-27 minutes, not observed in the EEMD. This oscillation, however, may not represent a fundamental mode but instead a harmonic related to the first longitudinal mode of oscillation whose period is ~55 minutes. We conclude that both methods were useful in helping to interpret the results of this study.

Keywords: *Monterey Bay, 2010 Chile Earthquake, Bay Response, Great Alaska Earthquake, spectral decomposition*

1. INTRODUCTION

When tsunamis from the open ocean enter coastal waters and embayments they often excite secondary oscillations whose periods are primarily determined by the boundaries that constrain them. Such oscillations are often referred to as free or natural oscillations or seiches. The natural oscillations of Monterey Bay have been a subject of study since the mid-1960s. The seiche modes of Monterey Bay were first examined by Wilson, Hendrickson, and Kilmer (WHK; 1965). They applied both analytical and numerical techniques using various simple geometrical shapes to approximate the bay in order to extract its natural modes of oscillation. In applying these methods, a nodal line was assumed to exist across the mouth of the bay from the Monterey Peninsula to Santa Cruz (Fig.1).

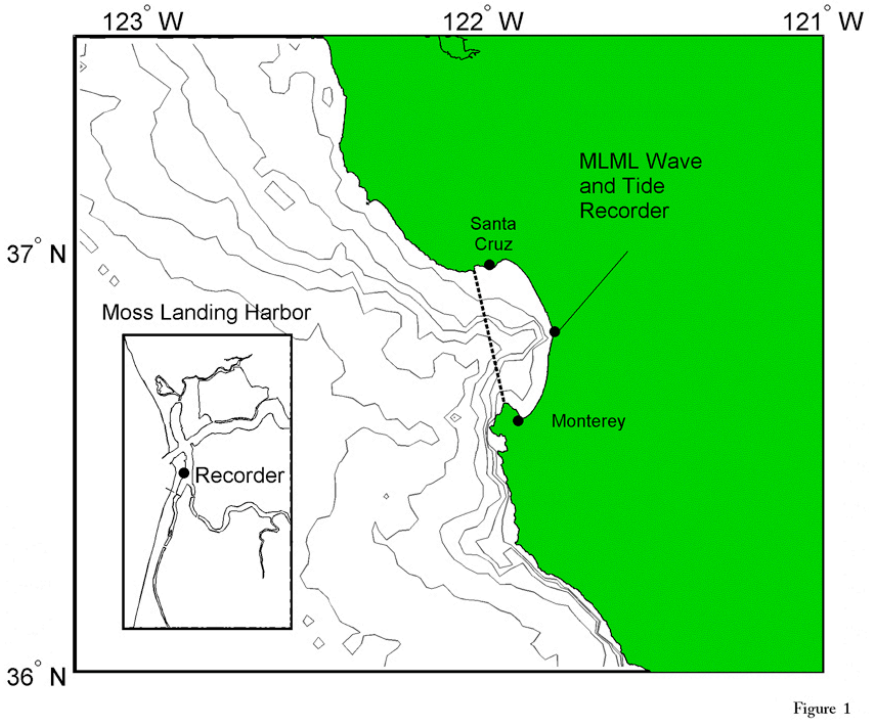

Figure 1. Map of the study area with an inset showing the location of the tide gauge in Moss Landing Harbor. The depth contours starting at the coast are 50, 100, 200, 500, 1000, and 2000 meters.

In describing the oscillating characteristics of the bay as a whole, we refer to the mode of oscillation oriented in the North-South direction as longitudinal, and the mode of oscillation oriented in the East-West direction as transverse. In addition to longitudinal and transverse modes of oscillation, WHK indicated that many higher modes of oscillation can be excited that are primarily restricted to certain parts of the bay including Monterey Harbor. Based on model results, they also found that the Monterey Submarine Canyon (MSC) separates the bay into two semi-independent halves with only weak coupling between them. Finally, periods were predicted for the lowest modes of oscillation in Monterey Bay with values of 44.2, 29.6, 28.2, 23.3, 21.6, and 20.4 minutes for the first 6 modes.

Subsequent studies have consistently shown natural periods of oscillation for the bay of approximately 55, 36, 27, and 21 minutes (e.g., Lynch, 1970; Breaker et al., 2008; Breaker et al., 2010), where an oscillation with a period of 55 minutes corresponds to the first longitudinal mode, and an oscillation with a period of 36 minutes corresponds to the first transverse mode. The response of Monterey Bay to the Loma Prieta Earthquake of 1989 and the Great Alaskan Earthquake of 1964 were recently examined by Breaker et al. (2009). They found that it is not clear how or where the tsunami associated with the Loma Prieta Earthquake was generated, but it occurred inside the bay and most likely began to take on the characteristics of a seiche by the time it reached the tide gauge in Monterey Harbor. Two primary periods of oscillation were found, one with a period 9-10 minutes, and the second with a period of 31-32 minutes. The first oscillation is in agreement with the range of periods for the expected natural oscillations of Monterey Harbor, and the second oscillation is consistent with a bay-wide oscillation or seiche mode. For the Great Alaskan Earthquake, which entered the bay across its mouth, several sequences of oscillations, all with a period of approximately 37 minutes, were found which corresponds to the transverse mode of oscillation. Finally, the sea level responses to these events differed greatly because different modes of oscillation were excited in each case.

Breaker et al. (2010) employed tidal data and numerical simulations to examine the oscillating characteristics of the bay. The model results were consistent with earlier studies, suggesting that the MSC separates the bay into two oscillating basins. However, water level and pressure data examined during the study indicated that oscillations corresponding to the four lowest natural frequencies (with periods of 55, 36, 27, and 21 minutes, respectively) tended to be bay-wide. Spatial patterns extracted from model-generated power spectra at the four lowest frequencies agreed closely with the modal patterns predicted by WHK. It was found that in addition to transient responses due to winter storm activity, low amplitude seiche oscillations occur on a continuous basis at the four lowest frequencies. Model simulations further indicated that both the winds and tides contribute to the oscillations.

The Chilean earthquake of 2010 occurred on February 27th at 06:34 UTC and lasted for approximately 90 seconds. The epicenter was located at 35.91°S, 72.73°W off the coast of central Chile at a depth of 35 km. The intensity of this event was 8.8 on the moment magnitude scale. This earthquake triggered a tsunami that spread across the Pacific basin. This event caused damage along the California coast at least as far north as San Diego. According to the Pacific Tsunami Warning Center, the observed maximum height of the tsunami at Monterey, California was 0.28 m with an arrival time of 20:31 UTC, almost 14 hours after the initial shock. An earthquake of magnitude 6.9 occurred approximately 90 minutes after the main event whose epicenter was located about 300km southwest of the location of the initial earthquake but may have not been related to it (U.S. Geological Survey, 2010).

In the present study, we examine water levels recorded during the Chilean earthquake of 2010 inside Monterey Bay to determine how the bay responded to this event. In the process, we compare the bay's response in this case with the bay's response to the Great Alaskan Earthquake of 1964. Our primary goal is to extract the frequency content of the tsunami-generated signals to determine what modes of oscillation were excited in Monterey Bay as a result of the Chilean earthquake of 2010. To accomplish this goal, we employ two methods of spectral decomposition, Singular Spectrum Analysis (SSA) and Ensemble Empirical Mode Decomposition (EEMD).

2. DATA ACQUISITION AND ANALYSIS

a. Data Acquisition

The water level data employed in this study were acquired in Moss Landing Harbor. Moss Landing is located almost equidistant from the north and south ends of Monterey Bay (Fig. 1). The instrument used to record the water level data is a SEA-BIRD Electronics SBE 26 Seagauge wave and tide recorder. The recorder is located next to the dock at the Moss Landing Small Boats Facility in Moss Landing Harbor (36.807°N, 121.788°W). The gauge is suspended from a piling one meter above the bottom. The measured water levels are thus directly proportional to the height of the water column directly above the gauge. The sampling interval is five minutes (0.0833 hours). As a result, the uncertainty in resolving the periods of interest (or any other period) is ± 2.5 minutes. The original record for the period from February 27 through March 6, 2010 is shown in Fig. 2.

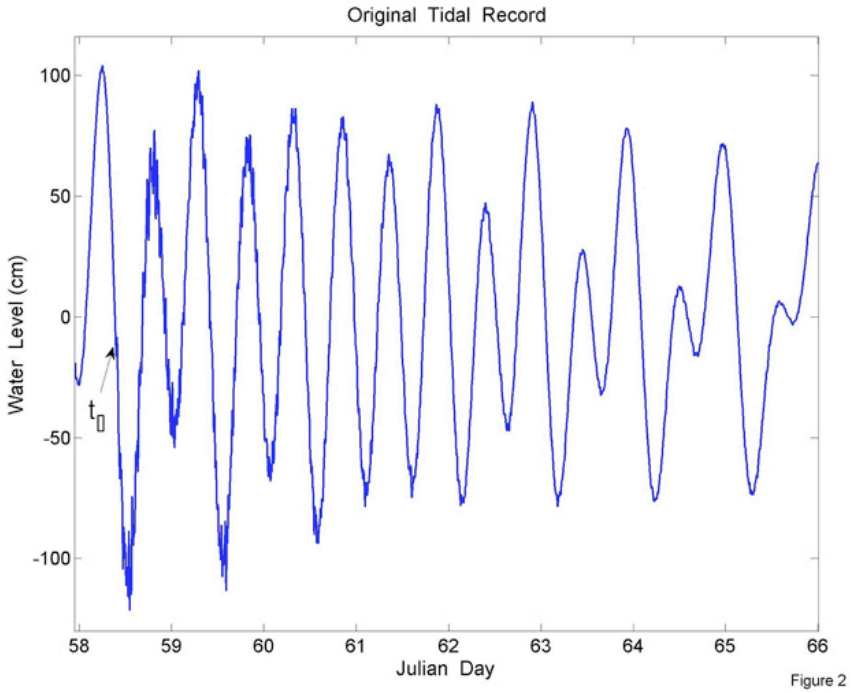

Figure 2. The original water level record acquired during the period of the Chilean earthquake of 2010 from the tide gauge in Moss Landing Harbor.

The first arrival is indicated by t_0 and, as stated above, occurs on Julian Day 58 at 06:34 UTC. Because the amplitude of this event is relatively small compared to the amplitude of the diurnal and semidiurnal tides in Monterey Bay it is difficult to observe in the original data. However, by using SSA and EEMD we were able to isolate and examine this event in detail.

b. Methods of Analysis

A primary objective of this study is to extract the frequency content of the tsunami-generated signals that were recorded in order to determine what modes of oscillation were excited in Monterey Bay from the Chilean earthquake of 2010. To determine the frequency content of these signals we have employed Singular Spectrum Analysis (SSA) and Ensemble Empirical Mode Decomposition (EEMD). Both methods decompose the data into a sequence of quasi-independent modes and are well suited for analyzing short, noisy records. In using SSA, the number of modes that the data are decomposed into is determined by the user whereas in EEMD, the number of modes is determined by the data. To illustrate the basic differences in how these methods are formulated, brief introductions to SSA and EEMD are given in Appendices A and B along with details concerning their implementation in this study.

3. RESULTS

a. Results from SSA

The Chilean earthquake of 2010 occurred on February 27th at 0634UTC. The recording at Moss Landing showed that this event lasted for at least four days before the amplitudes of all tsunami-related arrivals had decreased to background levels. In applying SSA to this record a window length (L) of 600 (600 x 0.08333 = 50 hours) was initially used. The eigenvalues are shown in the upper panel of Fig. 3. They represent the variance associated with each mode and, by convention, are plotted in descending order. The eigenvalues are plotted on a logarithmic scale in deciBels (dB). The first two eigenvalues form a pair that represents a single oscillation where the corresponding eigenvectors and principal components are in quadrature. The same is true for the 3rd and 4th eigenvalues. The first pair corresponds to the semidiurnal tide and the second to the diurnal tide. In order to examine the modes of interest in greater detail we have subtracted the reconstructed components for the first four modes to remove the influence of the tides and then subjected the residuals to SSA, in this case using a window length of 12 (12 x 0.08333 = 1 hour). Following the terminology of Golyandina et al. (2001), we refer to the results of this decomposition as Sequential SSA. The results are shown in the lower panel of Fig. 3.

Next, we examine the reconstructed components (RCs) from the Sequential SSA (Fig. 4). The vertical axes are expressed in cm and the x-axis extends from Julian Day 58 (February 27, 2010 to Julian Day 66 (March 7, 2010). First, we have summed RCs 1-4 to compare the maximum amplitude of the tsunami arrivals with that reported by the Pacific Tsunami Warning Center (PTWC). We obtain a maximum amplitude of approximately 20 cm compared to 28 cm reported by the PTWC. Our value

is somewhat lower and could be due in part to the fact that the value reported by the PTWC was obtained from the tide gauge in Monterey Harbor located almost 20 km SSW of Moss Landing.

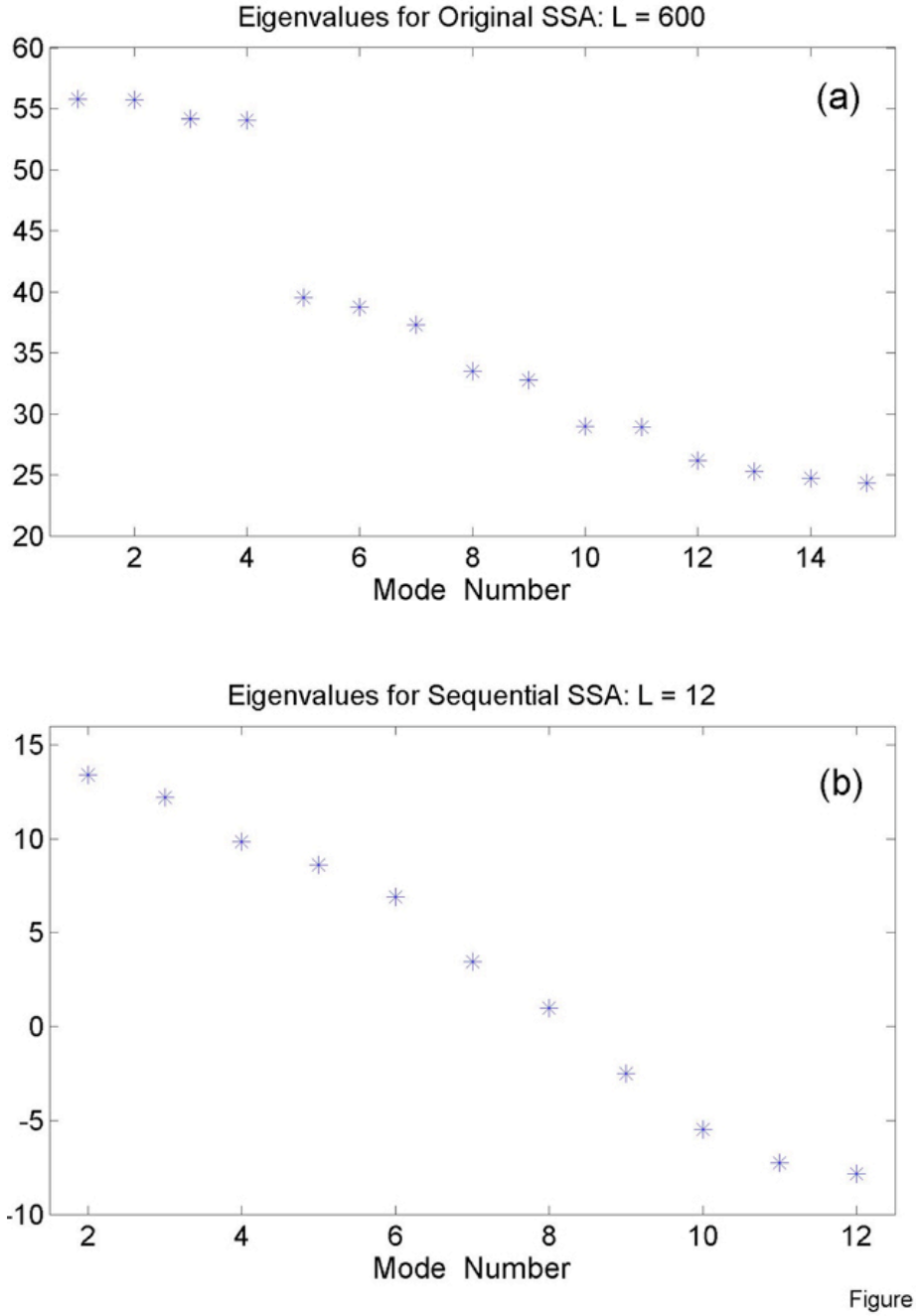

Figure 3

Figure 3. Eigenvalues from Singular Spectrum Analysis (SSA) for the original decomposition using a window length of 600 (50 hours) in the upper panel (a), and the eigenvalues from SSA after removing the first four reconstructed components from the original decomposition in the lower panel (b). The vertical axis is plotted on a logarithmic scale in deciBels (dB).

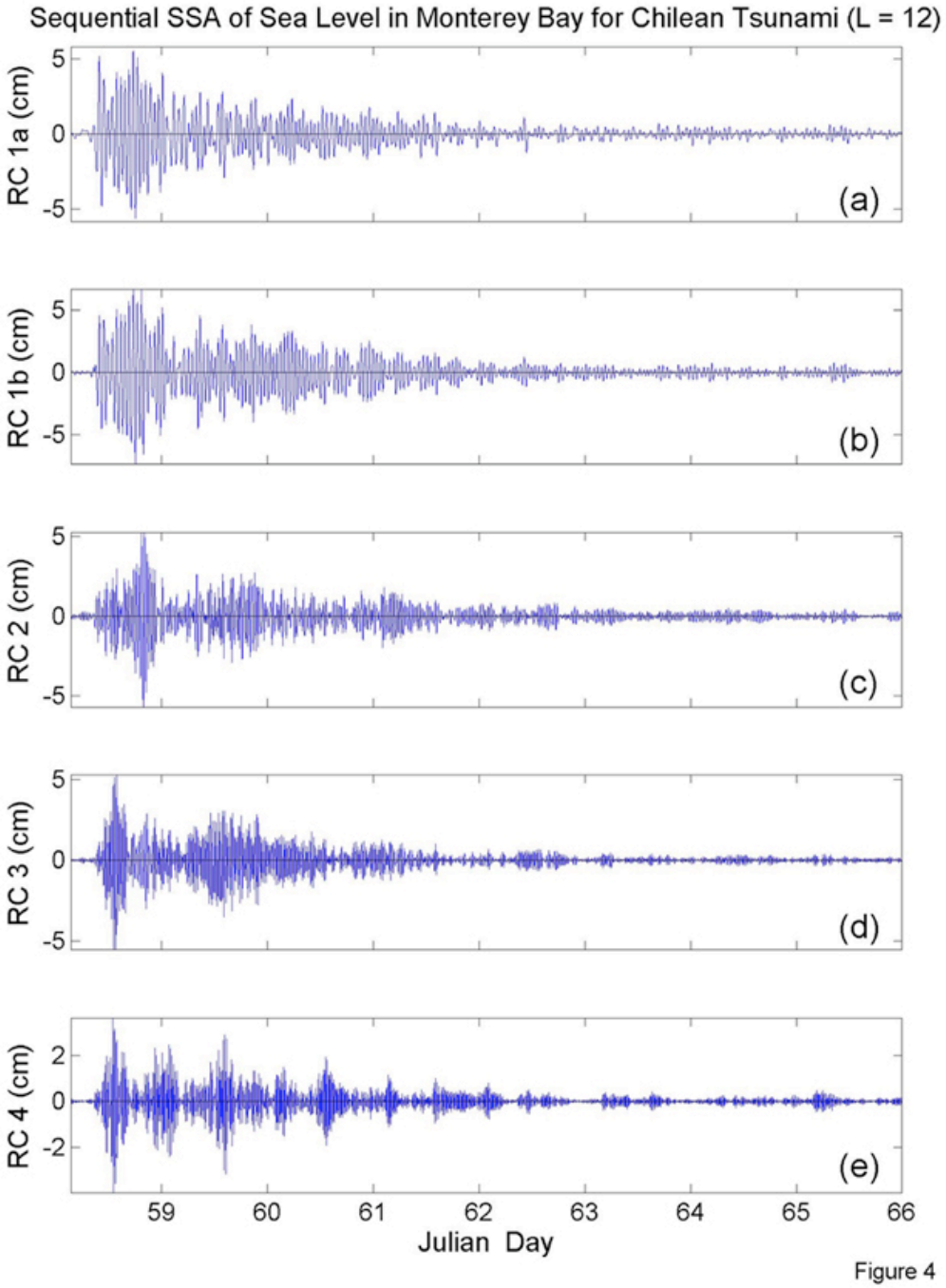

Figure 4

Figure 4. Reconstructed components (RCs) from the sequential SSA using a window length of 12 for Julian Days 58 through 65 showing an oscillation with periods of ~55 minutes (RCs 1a and 1b) in the top two panels (a & b), RC from the sequential SSA showing an oscillation with a period of 34-35 minutes (RC 2) in the third panel (c), RC from the sequential SSA showing an oscillation with a period of 26-27 minutes (RC 3) in the fourth panel (d), RC from the sequential SSA showing an oscillation with a period of 21-22 minutes (RC 4) in the fifth panel (e).

Continuing, we now examine the RCs or partial time series for frequency content. We found that the periods varied somewhat according to the number of modes that the data were originally decomposed into, and according to where in the arrival sequence we measured the periods. The first observation comes as no surprise since we expect that as L is increased, the effective bandwidth of each mode is decreased and so the variation in frequency is constrained to become smaller. After some experimentation we settled on a window length of 12 (1 hour) and have used this value throughout the analysis. Perhaps the most compelling reason for choosing this window length, however, is that it matches the number of Intrinsic Mode Function components (IMFs) that were obtained in the subsequent EEMD decomposition where the number of IMFs is determined by the data and so is not a free parameter chosen by the user. The second issue was more problematic but if any systematic patterns in the periods over an arrival sequence could be found it was that they tended to decrease slightly further into the sequence. What we report, however, are mean values estimated from samples taken at different locations throughout the sequence over the first 4 days. To summarize, RCs 1a and 1b produced a period with a mean value that falls between 52 and 57 minutes. In this case, there was a rather clear trend toward slightly shorter periods, as measurements were made further into the arrival sequence. We note that a period of approximately 55 minutes corresponds closely to the expected period for the first longitudinal mode of oscillation in Monterey Bay. The second RC has a period of 34-35 minutes and is close to the expected period for the first transverse mode of oscillation for Monterey Bay (~36 minutes). The third RC has a mean period of 26-27 minutes and has previously been observed on several occasions (e.g., Lynch, 1970). The fourth RC has a mean value of 21-22 minutes and is in close agreement with the value predicted by WHK (21.6 minutes) and observed in other studies (e.g., Breaker et al., 2008; Breaker et al., 2010). The results from the SSA decomposition are summarized in Table 1 below.

Returning to Fig. 3, the eigenvalues for the first two modes represent a single (well-defined) oscillation since the corresponding eigenvectors and principal components are in quadrature (not shown). However, the next three modes do not represent pure oscillations since they each correspond to a different frequency (Fig. 4). The explanation for this is that in the first case for oscillations with a period of approximately 55 minutes, there are approximately 11 samples per cycle for a sampling interval of 5 minutes, producing a waveform that closely approximates a pure sinusoid. However, for the next three modes with periods of 34-35, 26-27, and 21-22 minutes, the number of samples per cycle decreases yielding waveforms that increasingly depart from a pure sinusoid. For a period of 21-22 minutes, for example, there are only about 4 samples per cycle yielding a waveform that is far from sinusoidal and much closer to a saw tooth pattern. Thus, the decomposition treats the shorter undersampled periods as separate frequencies rather than oscillatory pairs.[1]

[1] Undersampling also made it more difficult to estimate the true periods of the oscillations in these cases.

Table 1. Period extraction using Singular Spectrum Analysis and Ensemble Empirical Mode Decomposition

Modal Sequence[1]	Singular Spectrum Analysis (SSA)	Ensemble Empirical Mode Decomposition (EEMD)	Comments
1	21 – 22 minutes	21 – 22 minutes	Previously predicted and observed
2	26 – 27	-------	May be 1st harmonic of 4th mode
3	34 – 35	-------	Close to observed transverse mode
4	57 –> 52[2]	55 –> 50[2]	Previously predicted and observed

[1] From shortest to longest periods.
[2] "–>" indicates that the period gets shorter further into the arrival sequence.

b. Results from EEMD

The results from the EEMD decomposition are shown in Fig. 5. The data are decomposed into 12 IMFs. Following Huang et al. (1998), the IMFs are ordered by frequency in descending order. The last IMF, IMF 12, in this case, is usually referred to as the residual and often corresponds to a long-term trend, if one exists. IMFs 3, 4, 5 and 6 contain the semidiurnal (IMFs 3 and 4) and diurnal (IMFs 5 and 6) tides. The higher modes are not of interest to us and so will not be discussed. Of primary interest are IMFs 1 and 2, which contain the tsunami-related signals. The separation between IMFs 2 and 3 is not complete as shown by the slight degree of mode mixing in IMF 3 during Julian Days 58 and 59. Although this reduces the variance in IMF 2, its impact is small and does affect the interpretation of our results. [2]

Analogous to the manner in which the eigenvalues are plotted by mode number in Fig. 3, we have plotted the variances for each IMF from EEMD in Fig. 6. The variances associated with the tsunami arrivals for IMFs 1 and 2 are small compared to the variances for the modes associated with the primary tidal constituents (IMFs 3, 4, and 5, and to a lesser extent, IMF 6), consistent with our interpretation of the eigenvalues shown in Fig. 3. The first two IMF components are plotted separately in Fig. 7 with the amplitudes expressed in cm. When IMF1 and IMF2 are combined, we obtain a peak amplitude of 22cm, close to the value obtained by summing the relevant RCs from SSA (20cm). The frequency analysis of IMF1 yields periods in the range of 21-22 minutes, virtually identical to the results we obtained from SSA. The second IMF (IMF2) yields periods in the range of 50-55 minutes,

[2] To ensure a level playing field in comparing SSA and EEMD, we also conducted EEMD using the residuals obtained from Sequential SSA and obtained almost the same results. However, there was slightly greater mode mixing between modes 2 and 3 and so we have not used the residuals from the SSA as the starting point for conducting EEMD.

similar, but not identical to the results we obtained for RC 4 from SSA. Again, there was a tendency for the periods to decrease slightly as measurements were made further into the arrival sequence between Julian Days 58 and 62. What we find particularly noteworthy are the absences of oscillations with periods of 26-27 minutes and 34-35 minutes, oscillations that were extracted using SSA. The results from the EEMD decomposition are summarized in Table 1.

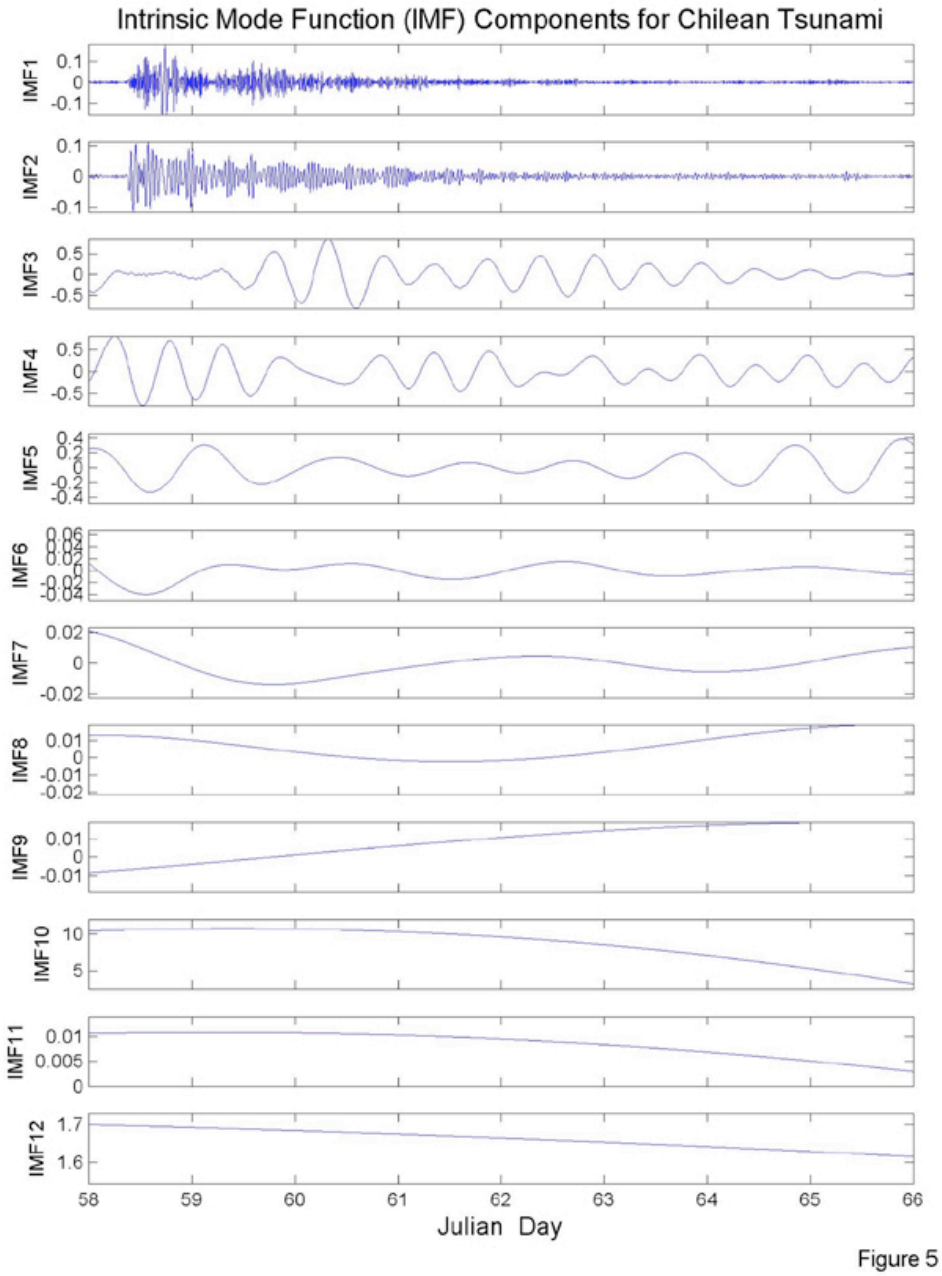

Figure 5. Intrinsic Mode Function Components (IMFs) from the EEMD decomposition. The first two IMFs (IMF1 and IMF2) show the wave trains for separate contributions from the Chilean earthquake.

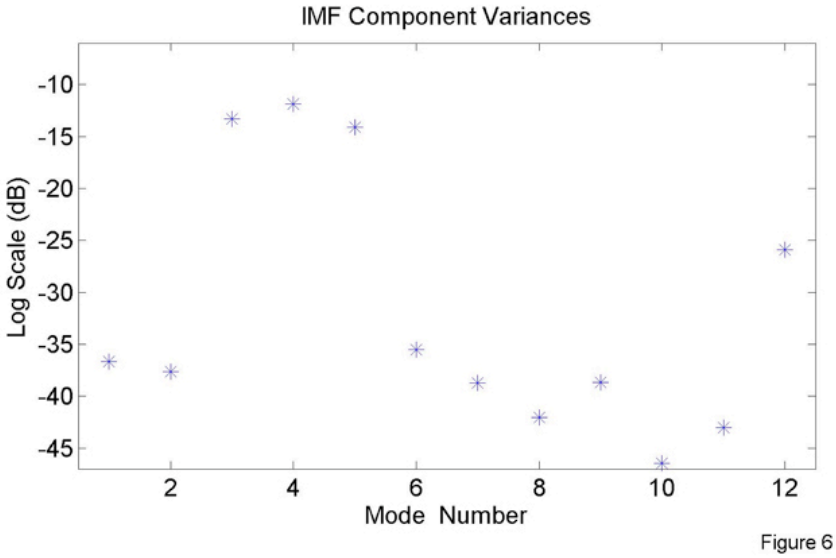

Figure 6. The variances are shown for each IMF component and are plotted in dB. The first two IMFs correspond to the variances associated with the first two IMF components shown in Fig. 5.

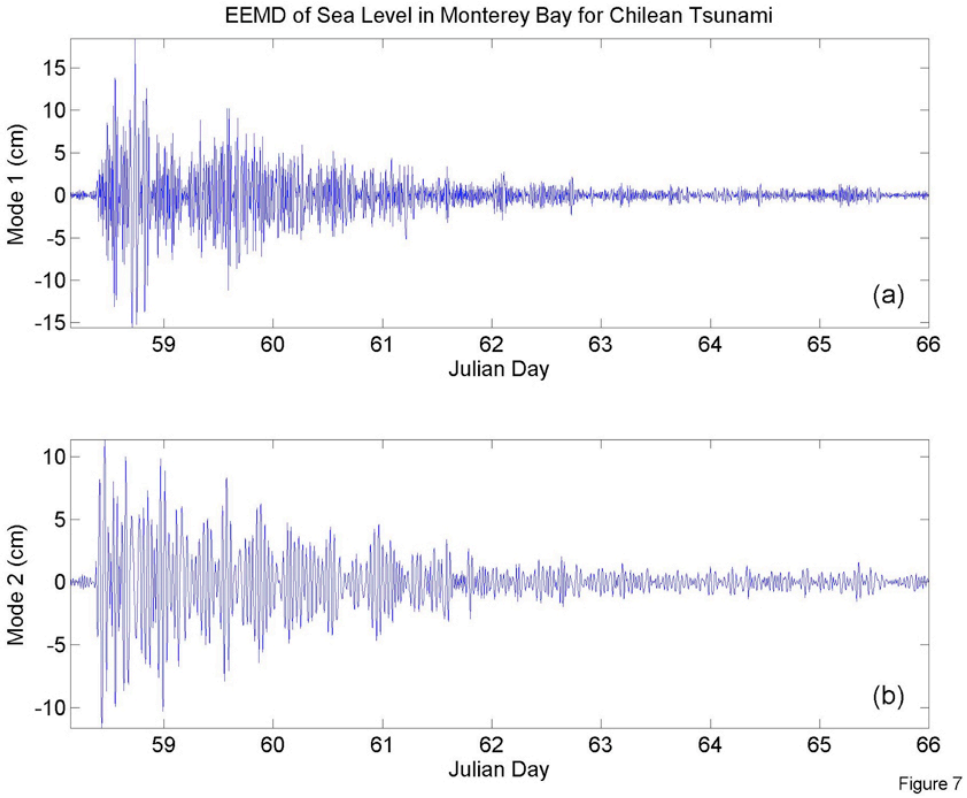

Figure 7. The first two IMF Components from the EEMD decomposition. The top panel (a) shows IMF1 with a primary period in the range of 21-22 minutes, and the bottom panel (b) shows IMF2 with a primary period in the range of 50-55 minutes.

c. Interpretation of the results

First we point out that the 6.9 magnitude earthquake that followed the main event by approximately 90 minutes may have contributed to the arrival sequence within the first few cycles since earthquakes with magnitudes that exceed 6.4 often produce tsunamis (Wilson, 1962). However, its impact must be considered small since it was far weaker than the main event.

The modal patterns for the frequencies associated with the natural oscillations of Monterey Bay were first predicted by WHK and more recently predicted and compared with observations by Breaker et al. (2010). RCs 1a and 1b from SSA and IMF2 from EEMD revealed periods in the range of 50-57 minutes consistent with the first longitudinal mode of oscillation for Monterey Bay. Model results from WHK and Breaker et al. (2010) suggest that MSC acts to separate the bay into two oscillating basins but water level data from Monterey and Santa Cruz (Fig. 1) indicate that the oscillations with the longest periods (55, 36, 27 and 21 minutes) span the entire bay. However, at higher frequencies, Breaker et al. (2010) concluded that MSC might serve as a more effective barrier. According to past observations, oscillations with periods of approximately 36 minutes correspond to the first transverse mode with a nodal line that is assumed to extend across the entrance of Monterey Bay (Fig. 1; Lynch, 1970; Breaker et al., 2008; Breaker et al., 2010). The results from SSA in response to the Chilean earthquake of 2010 reveal an oscillation with a period of 34-35 minutes, very close to this value. Breaker et al. (2009) in their examination of Monterey Bay's response to the Great Alaskan Earthquake of 1964 found that the resulting oscillations all had a period of approximately 37 minutes, consistent with an ocean wave that enters the bay across the entrance. As the wave enters Monterey Bay it conforms to the bay's dimensions and in the process is transformed into a seiche with a period that has been approximately predicted and closely observed on previous occasions. It was also noted that an oscillation with a node across the mouth of the bay and an antinode near Moss Landing is clearly reminiscent of quarter wave resonance. RC 3 from the SSA revealed a period 26-27 minutes. Observations with periods in this range have been previously reported but the true source of this oscillation is open to question. We discuss this issue in greater detail in section 4. Finally, SSA revealed a period of 21-22 minutes, which has been predicted by WHK and observed on numerous occasions. Its predicted spatial pattern spans the entire bay with antinodes at each end and a third antinode located at the center of the bay near Moss Landing.

As indicated earlier, IMF1 from EEMD revealed periods in the range of 21-22 minutes consistent with our results from SSA. IMF2 revealed periods in the range of 50-55 minutes, generally consistent with our results from SSA (52-57 minutes). In both cases, the periods tended to become shorter further into the arrival sequence, creating a signal that is slightly frequency modulated. Whether or not these variations simply reflect measurement uncertainties or are real is not clear, but emphasize the difficulties that arise in trying to estimate these periods.

Returning to Figs. 4 and 7, oscillatory behavior can be detected in the tsunami-generated signals for at least four days following the first arrival on Julian Day 58. As stated in Camfield (1980), the actual form of the wave train is initially determined by the generating mechanism, which includes the area of the uplifted sea bottom, the height and variation of the uplifted area, the depth of water, and related characteristics of the generating area. Between the epicenter and the observing site, multipath effects also spread the arrival pattern over time. As we examine each figure we see that the wave trains consist of arrival packets or groupings where the signal amplitudes are higher for periods

of several hours or longer and often repeat out to Julian Days 62 or 63 where the amplitudes finally decay to background levels. These extended or secondary oscillations may include reflections from outside or inside the bay, secondary undulations and/or energy trapping. Because the epicenter was located near the coast of Chile there are no obvious major reflecting boundaries between the epicenter and Monterey Bay in the eastern Pacific that would appear to contribute to the observed arrival sequence. If we are correct, then the observed arrival patterns are primarily due to processes that occur inside the bay. The arrival patterns in Figs. 4 and 7 in most cases display at least some degree of amplitude modulation. In Figs. 4e (RC 4) and 7b (IMF 2) the modulation patterns tend to be cyclic with periods of roughly 14 and 9 hours, respectively, indicating constructive reinforcement at preferred times.

Next we consider the importance of secondary undulations. Secondary undulations are oscillations whose periods correspond to the normal modes of a particular embayment that can be excited by several mechanisms including tsunamis (Kowalik and Murty, 1993). In most cases, they can be classified as one of three types, A, B, or C, depending on the geometry of the bay (Nakano, 1932). In type A, the secondary undulations appear as coherent wave trains with approximately the same waveform. In type B, they are not as regular and coherent as in type A, but are not completely irregular. In type C, the arrival patterns are essentially irregular. The type of secondary undulations can be roughly determined by plotting the depth of the bay versus $10S/b^2$, where S corresponds to the surface area of the bay, and b, its width. Monterey Bay has a length of approximately 40 km and a width of approximately 20 km and so has a surface area, S, of roughly 800 km^2. With an average depth of 100m, the secondary undulations fall into category B, where they are not as regular and coherent as in type A, but are not completely irregular. This result is generally consistent with the oscillatory patterns exhibited, but is, to some degree, mode dependent. This result is also consistent with a similar analysis performed by Breaker et al. (2009) for Monterey Bay who found that the wave trains associated with the Loma Prieta earthquake of 1989 and the Great Alaskan Earthquake of 1964 produced patterns consistent with type B.

Finally, we consider energy trapping as a third process that may contribute significantly to the observed arrival sequences. Energy trapping can take place along continental shelves and details concerning the types of wave motion that can be supported under such conditions are given in Murty et al. (2005) and Murty et al. (2008). Edge waves are one of several types of waves that can occur along continental shelves. Seiches have been known to produce edge waves in several cases (e.g., Murty et al., 2006). In certain situations, the energy associated with a given seiche mode can excite edge waves with the same period. Edge waves occur in the infragravity wave frequency band and significant energy has been observed in the shallow reaches of Monterey Bay in this range (MacMahan et al., 2004a; MacMahan et al., 2004b).

The following relationship given by Yanuma and Tsuji (1998) predicts the period, T, of a standing edge wave

$$T(M,L,a) = 2\pi\sqrt{2L}/\sqrt{(2M+1)\cdot\pi\cdot a\cdot g} \qquad (1)$$

where M is the mode number, L, the shelf width, a, the shelf slope, and g, the acceleration due to gravity. The shallow shelf regions in Monterey Bay extend roughly from Monterey Harbor to Moss Landing and out to the southern rim of MSC in the southern half of the bay, and from Moss Landing

up to Santa Cruz out to the northern rim MSC in the northern half of the bay (Fig. 1). We have selected a representative range of values for L and a for the first two edge wave modes (M=0 and M=1) and plotted $T(M,L,a)$ in each case (Fig. 8). For a shelf width of 5 km and a shelf slope of 0.01, for example, we obtain predicted edge wave periods in the range of 23–42 minutes. These wave periods are well within the range of periods associated with the natural oscillations of Monterey Bay and so energy trapping in the form of edge waves may occur and thus contribute to the arrival sequence observed in Figs. 4 and 7. However, we note that the extent to which energy trapping contributes to edge wave activity in Monterey Bay their occurrence will be restricted to the near shore regions and so our ability to observe them will depend strongly on location.

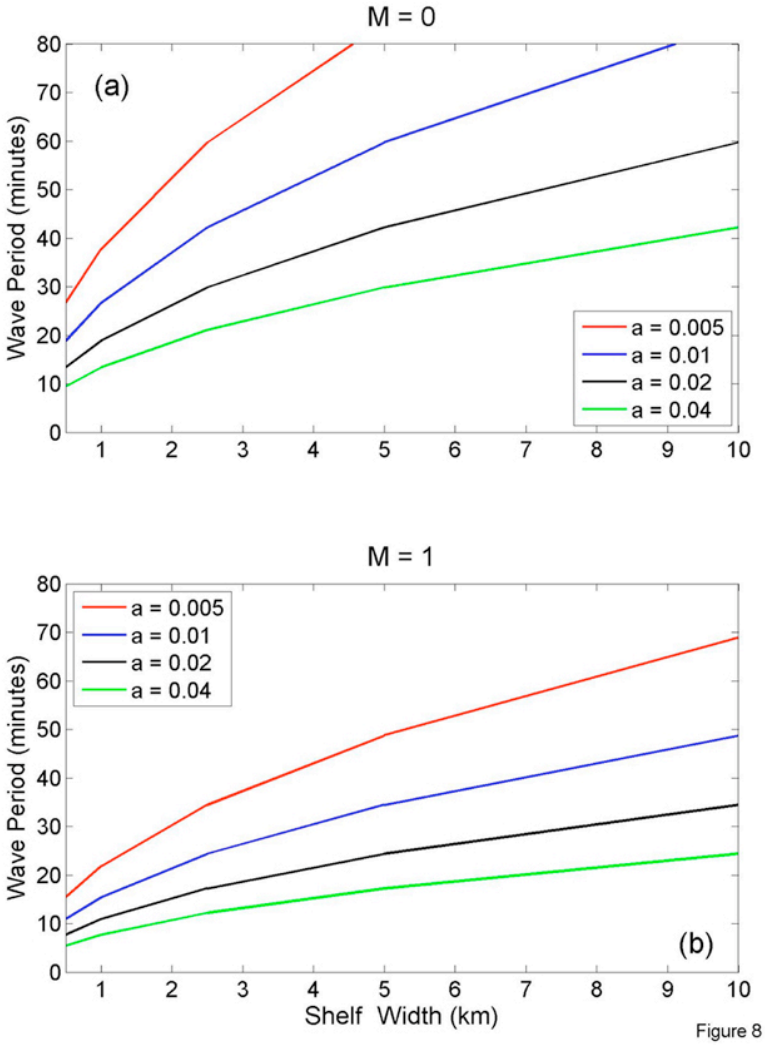

Figure 8. The predicted wave periods (in minutes) are shown for edge wave modes M = 0 in the top panel (a), and M = 1 in the lower panel (b). The wave periods are plotted as a function of shelf width in km along the abscissa, and bottom slope (a) for slopes of 0.005 (red), 0.01 (blue), 0.02 (black), and 0.04 (green).

4. DISCUSSION

Although the tsunamis generated by the Great Alaskan Earthquake of 1964 and the Chilean earthquake of 2010 both entered Monterey Bay across its mouth, the response to each event was quite different. In the first case, the Great Alaskan Earthquake excited only one mode, the first transverse mode of oscillation for Monterey Bay with a well-documented period of approximately 36 minutes consistent with quarter wave resonance. In the second case, the Chilean earthquake of 2010 excited several modes including the first longitudinal mode with a period in the neighborhood of 55 minutes. Both SSA and EEMD revealed this mode. SSA also revealed what is most likely the first transverse mode of oscillation with a period of 34-35 minutes although this mode was not detected in the EEMD decomposition. An oscillation with a period of 26-27 minutes was also detected in the SSA decomposition but its true nature has not been firmly established. Finally, both SSA and EEMD revealed an often-observed oscillation with a period of 21-22 minutes.

The tsunamis associated with the Great Alaskan Earthquake and the Chilean Earthquake both entered Monterey Bay from offshore but arrived from opposite directions. Unlike the Great Alaskan Earthquake, which excited only one resonant mode inside the bay, the Chilean Earthquake excited several modes. The bay's response to these two tsunamis was very different and must be related to the manner in which the tsunami-generated waves associated with these events entered the bay. First, as discussed by Defant (1961), the period of the longest free oscillation that enters an embayment is expected to increase significantly for embayments with relatively wide entrances. For a simple rectangular bay with a flat bottom where the width of the entrance is equal to its length, the period will be increased by approximately 37%. For Monterey Bay, the width of the entrance actually exceeds the distance between the entrance and Moss Landing by at least 35% and so considerable period lengthening is expected. Also, the shape of the entrance to an embayment has a great effect on the period of incoming free oscillations, according to Defant (1961). The shape of the entrance to Monterey Bay is somewhat asymmetric due to the presence of the Monterey Peninsula at the southern end of the bay (Fig. 1). Breaker and Broenkow (1994) found that poleward propagating disturbances along the coast took almost 5 days to travel from a point approximately 10km north of Pt. Sur on the open coast (Fig. 1) to a point located inside the bay at its southern extremity, suggesting that propagating waves from the south take a rather circuitous path into the bay. Conversely, incoming waves from the north should enter the bay via a more direct path where the coastline is less obstructed. Further, according to Murty (1984), the direction from which a tsunami approaches the entrance to a bay determines to a large extent the amplitudes, frequencies, and phases of the oscillations inside the bay. As a result we expect that there will be a preferred direction for which maximum amplitudes of the resonant modes inside the bay will occur. Thus, we conclude that (1) the period of incoming tsunami-generated waves (regardless of the direction from which they arrive) will be increased significantly due to the relatively wide entrance, (2) the asymmetric shape of the entrance to Monterey Bay may affect the periods of incoming tsunami-generated waves differently for those that enter the bay from the south than for those that enter from the north, and (3), the directions of the incoming waves were most likely different in each case.

The Great Chilean or Valdivia Earthquake of May 22, 1960 was the most powerful earthquake ever recorded, measuring 9.5 on the moment magnitude scale. It generated a tsunami that affected most of the greater Pacific basin from Chile to Alaska. However, we have no record of this event in

Monterey Bay, since, to our knowledge, no tide gauge was in operation at that time. Because the epicenter of the Valdivia Earthquake was located along the coast of Chile similar to the Chilean earthquake of 2010, although several hundred km further south, the seiche modes excited by this event in Monterey Bay may have been similar although the amplitudes were most likely much higher and the arrival sequence may have lasted longer.

Next we consider the seiche mode whose period is approximately 27 minutes. It roughly corresponds to the third mode of oscillation predicted by WHK with a period of 28 minutes but its corresponding spatial pattern was confined to the southern half of the bay, not consistent with subsequent bay-wide observations at this frequency. According to Lynch (1970), an oscillation with a period of 27 minutes could correspond to a shelf wave, and results from this study suggest that energy trapping in the shallow shelf areas of Monterey Bay could lead to the formation of edge waves with periods of this order. However, Breaker et al. (2008), using EEMD applied to water levels in Elkhorn Slough detected modes of oscillation with periods of approximately 55, 36, 27, and 22 minutes using conventional spectral analysis but did not detect an oscillation with a period of 27 minutes using EEMD. This result is consistent with our results from this study using EEMD. As discussed in Huang et al. (1998), because EEMD is not based on Fourier methods of decomposition, the energy associated with nonlinearities in the data is not represented by harmonics but takes a different form.[3] Thus, the question arises as to whether a spectral maximum with a period of approximately 27 minutes represents a fundamental oscillation or simply a harmonic? Based on our experience with EEMD we favor the latter explanation.

Finally, different results were obtained using SSA and EEMD. SSA detected oscillations with periods of 52-57 minutes, 34-35 minutes, 26-27 minutes, and 21-22 minutes, whereas EEMD detected oscillations with periods of 50-55, and 21-22 minutes. The slight differences in the first case can most likely be attributed to measurement uncertainties. These uncertainties include actual changes in the period of oscillation dependent on where in the arrival sequence the measurements were made, uncertainties due to the sampling interval, and finally, differences due to bandwidth considerations. Although the results of EEMD did not reproduce an oscillation in the range of 34-35 minutes, in our past experience in comparing these methods, we have detected certain oscillations using EEMD that were not detected using SSA and so, in our view, the jury is still out on whether one method is inherently better than the other in its ability to resolve different oscillations. As discussed above, SSA detected an oscillation with a period in the range of 26-27 minutes but its reality is seriously in doubt. Finally, both methods detected an oscillation with a period of 21-22 minutes.

5. SUMMARY AND CONCLUSIONS

The purpose of this study has been to extract the primary frequencies contained in the arrival sequence produced by the tsunami from the Chilean earthquake of 2010 in order to determine what

[3] Breaker et al. (2008) found that the energy associated with harmonics in conventional spectral analysis appeared to be rather uniformly distributed across a broad range of frequencies in the corresponding EEMD analysis based on the Hilbert spectrum.

natural oscillations or seiche modes were generated in Monterey Bay. Two methods of spectral decomposition, Singular Spectrum Analysis (SSA) and Ensemble Empirical Mode Decomposition (EEMD), were employed to extract the frequencies of interest and provided a useful basis for comparison. Although the amplitudes of the tsunami-generated signals were small in comparison to the semidiurnal and diurnal tides, by using SSA and EEMD we were able to effectively separate the signals of interest for detailed examination. The wave train associated with of the Chilean tsunami lasted for at least four days in Monterey Bay due to several processes. It was concluded that although reflections may not have contributed significantly to the arrival sequence, secondary undulations, and energy trapping in the form of edge waves, most likely did contribute to the tsunami-related arrivals.

The results of the SSA decomposition resolved oscillations with periods of 52-57, 34-35, 26-27, and 21-22 minutes, all frequencies that have been predicted and/or observed in previous studies. The results of the EEMD decomposition only detected oscillations with periods of 50-55, and 21-22 minutes. Periods in the range of 50-57 minutes were somewhat variable due to measurement uncertainties but almost certainly correspond to the first longitudinal mode of oscillation for Monterey Bay (e.g., Breaker et al., 2010). Periods in the range of 34-35 minutes correspond to the first transverse mode of oscillation that assumes a nodal line across the entrance of the bay. A period of approximately 37 minutes, close to the period of 34-35 minutes observed in this study, was observed from the Great Alaskan Earthquake of 1964 in Monterey Bay and most likely represents the same mode of oscillation. A period in the range of 26-27 minutes, although previously observed, does not necessarily represent a fundamental mode (Breaker et al., 2008), and a period in the range of 21-22 minutes has been predicted and observed on several occasions (e.g., Lynch, 1970). The tsunamis associated with the Great Alaskan Earthquake and the Chilean Earthquake both entered Monterey Bay from offshore but from opposite directions. Unlike the Great Alaskan Earthquake, which excited only one resonant mode inside the bay, the Chilean Earthquake excited several modes suggesting that the asymmetric shape of the entrance to the bay was an important factor, and that the directions of the incoming tsunami-generated waves were most likely different.

Finally, the results from SSA and EEMD produced somewhat different results. Although a period of 34-35 minutes was observed in the results from SSA, it was not detected in the results from EEMD. However, in previous comparisons between the two methods we have observed that oscillations detected in EEMD were not obtained using SSA. SSA also revealed an oscillation with a period of 26-27 minutes, not observed in the results from EEMD. As pointed out above, however, this oscillation may not represent a fundamental mode but instead may be harmonically related to the first longitudinal mode of oscillation whose period is approximately 55 minutes. Overall, both methods have been helpful in interpreting the results of this study.

REFERENCES

Breaker, L.C., and W.W. Broenkow (1994), The circulation of Monterey Bay and related processes. Oceanography and Marine Biology: an Annual Review, 32, 1-64.

Breaker, L.C., W.W. Broenkow, W.E. Watson, and Y.-H. Jo (2008), Tidal and non-tidal oscillations in Elkhorn Slough, California. Estuaries and Coasts, 31, 239 – 257.

Breaker, L.C., T.S. Murty, J.G. Norton, and D. Carroll (2009), Comparing the sea level response at Monterey, California to the Loma Prieta Earthquake of 1989 and the Great Alaskan Earthquake of 1964. Science of Tsunami Hazards, 28, 255 - 271.

Breaker, L.C., Y.-H. Tseng, and X. Wang (2010), On the natural oscillations of Monterey Bay: observations, modeling, and origins. Progress in Oceanography, 86, 380-395, doi: 10:1016/j.pocean.2010.06.001.

Camfield, F.E. (1980), Tsunami Engineering. Special Report No. 6. U.S. Army, Corps of Engineers, Coastal Engineering Research Center, Fort Belvoir, VA, 222 pp.

Defant, A. (1961), Physical Oceanography: Volume II. The MacMillan Company, New York.

Flandrin P., G. Rilling G, and P. Concalves (2004), Empirical mode decomposition as a filter bank. IEEE Signal Processing Letters, 11, 112 – 114.

Ghil, M., M.D. Allen, K. Dettinger, D. Kondrashow, M.E. Mann, A.W. Robertson, A. Saunders, Y. Tian, F. Varadi, and P. Yiou (2002), Advanced spectral methods for climatic time series. Reviews of Geophysics, 40, 1003, 3-1 – 3-41.

Golyandina, N., V. Nekrutkin, and A. Zhigljavsky (2001), Analysis of Time Series Structure: SSA and Related Techniques. Monographs on Statistics and Applied Probability 90. Chapman & Hall/CRC, Boca Raton.

Huang, N.E., and others (1998), The empirical mode decomposition and the Hilbert spectrum for nonlinear and non-stationary time series analysis. Proceedings of the Royal Society of London A, 454, 903- 995.

Huang, N.E. (2005a), Introduction to the Hilbert-Huang Transform and its related mathematical problems, p. 1-24. In: Huang NE, Shen SSP (eds) Hilbert-Huang Transform and its applications, Interdisciplinary Mathematical Sciences - Vol. 5. World Scientific, New Jersey.

Huang, N.E. (2005b), Introduction to the Hilbert-Huang Transform and some recent developments,. In: Huang NE, Attoh-Okine NO (eds) Hilbert-Huang Transform in Engineering. Taylor & Francis, Boca Raton. pp 1-24.

Jenkins, G.M., and D.G. Watts (1968), Spectral Analysis and its Applications. Holden-Day, San Francisco.

Kowalik, Z., and T.S. Murty (1993), Numerical Modeling of Ocean Dynamics. World Scientific, Singapore.

Lynch, T.J. (1970), Long wave study of Monterey Bay. M.S. Thesis, Naval Postgraduate School, Monterey, California.

MacMahan, J.H., J.H. Reniers, E.B. Thornton, and T.P. Stanton (2004a), Infragravity rip current pulsations. Journal of Geophysical Research, 109, C01033, doi: 10.1029/2003JC002068.

MacMahan, J.H., J.H. Reniers, E.B. Thornton, and T.P. Stanton (2004b), Surf zone eddies coupled with rip current morphology. Journal of Geophysical Research, 109, C07004, doi: 10.1029/2003JC002083.

Murty, T. S. (1984), Storm Surges – Meteorological Ocean Tides. Bulletin Number 212. Canadian Journal of Aquatic Sciences, 897 pages.

Murty, T.S., N. Nirupama, I. Nistor, and A.D. Rao (2005), Role of trapped and leaky modes around Andaman and Nicobar Islands: Tsunami of 26 December 2004. Proceedings of the National Workshop on Tsunami Effects and Mitigation Measures, Allied Publishers Pvt. Ltd., Chennai, pp. 3-21.

Murty, T.S., U. Aswathanarayana, and N. Nirupama (2006), The Indian Ocean Tsunami. Taylor & Francis, London.

Murty, T.S., N.P. Kurian, and M. Baba (2008), Roles of reflection, energy, trapping and secondary undulations in the tsunami on Kerala coast. International Journal of Ecology & Development, 10, 100-114.

Nakano, M. (1932), Preliminary note on the accumulation and dissipation of the energy of secondary undulations in a bay. Proc. Phys. Math. Soc. Japan, SER 3, 44-56.

Peel M.C., G.E. Amirthanathan, G.G.S. Pegram, T.A.McMahon, and F.H.S. Chiew (2005), Issues with the application of Empirical Mode Decomposition analysis. In: Zerger, A., Argent R.M. (eds) MODSIM 2005 International Congress on Modelling and Simulation, Modelling and Simulation Society of Australia and New Zealand, December 2005, pp 1681-1687.

Preisendorfer, R.W. (1988), Principal Component Analysis in Meteorology and Oceanography. Elsevier, Amsterdam.

United States Geological Survey (2010), USGS, Earthquake Hazards Program (March 6, 2010). "10-Degree Map Centered at 35S, 75W".

Vautard, R., P. Yiou, and M Ghil (1992), Singular-spectrum analysis: A toolkit for short, noisy chaotic signals. Physica D, 58, 95-126.

Wilson, B.W., J.A. Hendrickson, and R.E. Kilmer (1965), Feasibility study for a surge - action model of Monterey, California. U.S. Army Corps of Engineers, Waterways Experiment Station, Vicksburg, MS, 166 pp.

Wilson, B. W. , L. M. Webb, and J. A. Hendrickson (1962), The nature of tsunamis: Their generation and dispersion in water of finite depth. NESCO Technical Report No. SN 57-2, National Engineering Science Company.

Wu, Z., and N. E. Huang (2009), Ensemble empirical mode decomposition: A noise-assisted data analysis method. Advances in Adaptive Data Analysis, 1, 1 – 41.

Yanuma, T. , and Y. Tsuji (1998), Observations of edge waves trapped on the continental shelf in the vicinity of Makurazaki Harbour, Kyushu, Japan. Jour. Oceanog., 54, 9-18.

APPENDIX A – SINGULAR SPECTRUM ANALYSIS

Singular Spectrum Analysis (SSA) is a method of spectral decomposition that is similar in many respects to Principal Component Analysis (e.g., Preisendorfer, 1988). According to Golyandina et al. (2001), the general purpose of SSA is to decompose a time series into a sum of a small number of interpretable components or modes such as a slowly varying trend, oscillatory components and "structureless"noise. The data adaptive nature of the basis functions that are employed in SSA make the method suitable for analyzing data that may be nonlinear and/or non-stationary. SSA can be applied to relatively short, noisy time series (e.g., Vautard et al., 1992), making it well suited for analyzing the data employed in this study.

To perform SSA, a multidimensional time series called the trajectory matrix is initially formed from the original one-dimensional time series. The dimension of this matrix is called the window length, L. As stated by Ghil et al. (2002), this process is equivalent to representing the behavior of the system by a succession overlapping views of the series through a sliding window whose length is equal to L. The trajectory matrix can be formed from a univariate time series in several ways. The approach we use leads to a Toeplitz trajectory matrix. A Toeplitz matrix is symmetric and has the property of being diagonally-constant with dimensions in this case of L x L. To construct a Toeplitz trajectory matrix, the lagged covariances, S_{ij} , for a time series x_t, , $t = 1,2,\ldots\ldots,N$, are calculated according to

$$S_{ij} = \frac{1}{N - |i - j|} \sum_{t=1}^{N-|i-j|} x_{|i-j|+t} x_t \qquad (1a)$$

where we have centered the record by first removing the mean. S_{ij} is equivalent to the unbiased version of the autocovariance function due to the normalization that is employed (Jenkins and Watts, 1968). The resulting matrix, $\boldsymbol{S}$, at this point can be decomposed into eigenvalues, λ_k and eigenvectors, e_k , according to

$$\Lambda = E^T S E \qquad (2a)$$

where $\boldsymbol{E}$ is the diagonalizing matrix whose columns contain the eigenvectors, $\boldsymbol{E^T}$, its transpose, and the elements of the diagonal matrix, $\boldsymbol{\Lambda}$, contain the eigenvalues. When the square roots of the eigenvalues or singular values are plotted in descending order, the so-called "singular spectrum" is obtained. The principal components, a_k, can be obtained by projecting the time series onto each eigenvector as

$$a_t^k = \sum_{j=1}^{L} x_{t+j} e_j^k \qquad (3a)$$

where $t = 1,2,\ldots,N$, and e_j^k represents the j^{th} component of the k^{th} eigenvector, and the number of principal components that are produced is equal to $N - L + 1$.

The principal components represent moving averages or filtered versions of the original series, x_t .

Finally, the original times series can be recovered by calculating the reconstructed components (Vautard et al., 1992). The k^{th} reconstructed component can be calculated according to

$$r_t^k = \frac{1}{F_t} \sum_{j=G_t}^{H_t} a_{t-j+1}^k e_j^k \qquad (4a)$$

where the lower and upper limits of summation, G_t and H_t , and the normalizing factor, F_t , depend on location within the time series. Following Ghil et al. (2002), the normalizing factor, $F_t = 1/t$, for $1 \le t \le L\text{-}1$, $1/L$, for $L \le t \le N - L + 1$, and $1/N\text{-}t+1$, for $N - L + 2 \le t \le N$. The lower limit, $G_t = 1$, for $1 \le t \le L\text{-}1$, 1, for $L \le t \le N - L + 1$, and $t\text{-}N+M$, for $N - L + 2 \le t \le N$. The upper limit, $H_t = t$, for $1 \le t \le L\text{-}1$, L, for $L \le t \le N - L + 1$, and L, for $N - L + 2 \le t \le N$. Unlike the principal components which have length $N - L + 1$, the reconstructed components have length N, equal to that of the original time series. These components correspond to partial time series and when summed over all modes reproduce the original time series within the accuracy of the calculations.

APPENDIX B – EMPIRICAL MODE DECOMPOSITION

The method we employ is referred to as Empirical Mode Decomposition and Hilbert Spectral Analysis, or EMD/HSA. More concisely, EMD/HSA is called the Hilbert-Huang Transform, or simply the HHT. The methodology is described in detail by Huang et al. (1998), Huang (2005a), and Huang (2005b). Unlike SSA which has a formal mathematical basis, EEMD is empirically based thus emphasizing the inherent differences in these methods.

In this study we focus on that portion of the methodology that involves EMD. EMD is a method of decomposing a time series into a sequence of empirically orthogonal Intrinsic Mode Function (IMF) components and a residual. The method is similar to Singular Spectrum Analysis (Golyandina et al., 2001). However, in EMD, the number of modes is determined by the data whereas in Singular Spectrum Analysis (SSA), the number of modes is determined by the user. EMD is data adaptive, and, in contrast to Fourier spectral decomposition, it does not require stationarity of the data. As such, it is well-suited for the analysis of non-stationary and nonlinear time series. The IMF components are often physically meaningful because the characteristic scales in each case are determined by the data itself. As in SSA, selected modes may require grouping in order to extract a physical basis. A number of recent studies have examined EMD in detail (Flandrin et al., 2004; Peel et al., 2005; Huang, 2005a; Huang, 2005b).[1]

Each IMF represents a mode of oscillation with time-dependent amplitude and frequencies that lie within a narrow band, the center of which defines the mean period of the mode. The process of extracting the individual modes or essential scales from the data is called sifting and is performed

[1] The last two references refer to texts that contain chapters by various authors.

many times to produce a single IMF. In this process local maxima and minima are identified in the record and envelopes are formed by fitting cubic splines to the extreme values. The differences between the envelope and the mean provide an estimate of the first IMF component. Once the first IMF, imf_1, has been obtained, it is subtracted from the original data, $x(t)$, producing residuals, r_1, which can be expressed as

$$x(t) - imf_1 = r_1 . \qquad (1b)$$

The residuals, r_1, are then subjected to the same process, yielding the second IMF, imf_2, as

$$r_2 = r_1 - imf_2 , \qquad (2b)$$

and so on, until a final residual is obtained that often corresponds to a long-term trend in the data.

One problem in the application of EMD is that mode mixing occurs when a time series includes intermittently occurring signals of widely separated time scales, i.e., when a high-frequency signal in one time interval is followed by a smooth, low frequency signal in the following time interval. To address this problem, Wu and Huang (2009) have developed a noise-assisted technique called "ensemble EMD", or EEMD, which defines the true IMF as the mean of an ensemble of IMFs. An ensemble member consists of the signal plus white noise. By creating an ensemble of IMFs, it is possible to generate IMFs, each of which has a narrow frequency band, that essentially do not overlap with the frequencies that are contained in adjacent IMFs. In applying the technique, the white noise that is added to the signal according to

$$x_i(t) = x(t) + \varepsilon_i(t) \qquad (3b)$$

where $x(t)$ represents the i^{th} observation, $x_i(t)$ represents the i^{th} observation perturbed by white noise, and $\varepsilon_i(t)$ represents the white noise that is added to the i^{th} observation. The amplitude of the added noise, $\varepsilon_i(t)$, can be calculated as the ratio of the standard deviation of the added noise to that of the input data. In our case we have used a value of 0.1, but we also initially used values of 0.05 and 0.20, and obtained similar results in each case. Typically, the number of realizations or ensemble size is several hundred in order to obtain $x_i(t)$. In the present study we used an ensemble size of 300 in each case. Finally, the maximum number of IMFs that can be generated from a given data set is approximately given by $Log_2(N)$, where N represents the total number of observations in the record. This upper limit is based on the fact that the number of zero-crossings from one IMF to the next decreases by a factor that is approximately one half. In practice, however, somewhat fewer IMFs are usually produced.